Acta Cryst. (1996). B52, 458–464

Charge Density Studies in $NH_4[Ti(C_2O_4)_2].2H_2O$ Crystals at Two Wavelengths

H. S. SHEU,[a,b] J. C. WU,[a] Y. WANG[a,b]* AND R. B. ENGLISH[c]

[a]*Department of Chemistry, National Taiwan University, Taipei, Taiwan,* [b]*Synchrotron Radiation Research Center, Hsinchu, Taiwan, and* [c]*Department of Chemistry, Rhodes University, South Africa*

(Received 30 May 1995; accepted 18 September 1995)

Abstract

The crystal structure of ammonium bis-μ-oxalato-titanate(III) dihydrate, $NH_4[Ti(C_2O_4)_2].2H_2O$, is reinvestigated by careful single-crystal X-ray diffraction using Mo $K\alpha$ (room temperature and 130 K) and Ag $K\alpha$ radiation (room temperature). It crystallizes in noncentrosymmetric hexagonal space group $P6_422$, with cell parameters a = 8.947 (2), c = 10.898 (1) Å, Z = 3, $F(000)$ = 423, M_r = 278.1, D_x = 1.833, R = 0.035, wR = 0.030 for 2296 observed reflections with $I \geq 2\sigma(I)$, on Ag $K\alpha$ data. Accurate data measurement was applied using two wavelengths (0.7107 Å for Mo $K\alpha$ and 0.5609 Å for Ag $K\alpha$) in order to study the charge density distribution and also to investigate the wavelength effect in such investigations. A total of 22 650 and 20 298 reflections were measured using Mo $K\alpha$ radiation at room temperature and 130 K, respectively, and 18 361 reflections using Ag $K\alpha$ radiation. The Ti atom is coordinated by four oxalate dianions with coordination number 8 in an approximate symmetry of D_4 geometry. Each oxalato ligand is bridged between two Ti atoms and forms an infinite polymeric spiral column along the c axis. The deformation density maps, $\Delta\rho$, obtained from all three data sets are consistent and agree well. Although the formal charge of Ti in this complex is 3+, with only one electron on the 3d orbitals expected, the net atomic charge on Ti from this study is ~2+. Charge asphericity around the Ti atom caused by the splitting of 3d orbitals is clearly observed in the deformation density. The d-orbital populations are evaluated from multipole refinement. The expected d^1 electron is mainly located in the d_{z^2} orbital.

1. Introduction

Complexes with high coordination number are becoming increasingly common and we are interested in determining the electronic configuration of d orbitals in such a crystal field. The oxalate dianion was found to be a common ligand for a few metal complexes with coordination number more than 6, such as Ti(7,8) (Eve & Niven, 1990; English & Eve, 1993; Drew & Eve, 1977*a*,*b*), Pb(7) (Christensen, Cox & Lehmann, 1989; Virovets, Naumov, Boldyreva & Podberezskaya, 1993), Cd(7) (Huang, Wang & Thomas, 1990), In(8) (Bulc, Golic & Siftar, 1983) and Ba(12) (Chaix-Pluchery, Mutin, Bouillot & Niepce, 1989); the numbers in parentheses are the coordination numbers. Magnetic exchange interactions of μ-oxalato binuclear complexes have been studied for many years (Julve, Verdaguer, Gleizes, Philoche-Levisalles & Kahn, 1984; Felthouse, Laskowski & Hendrickson, 1977; Curtis, Ross, McCormick & Waters, 1973). Recently, oxalato-bridged heterometallic complexes have been designed as ferromagnetic materials, $\{NBu_4[M^{II}Cr^{III}(ox)_3]\}_x$ [M^{II} = Mn, Fe, Co, Ni, Cu, Zn (Ohba, Tamaki, Matsumoto & Okawa, 1993; Tamaki, Zhong *et al.*, 1992; Zhong, Matsumoto, Okawa & Kida, 1990)], and ferrimagnets, $\{NBu_4[M^{II}Fe^{III}(ox)_3]\}_x$ [M^{II} = Mn, Fe, Ni, Zn (Tamaki, Mitsumi *et al.*, 1992)]. Here, the D_3-symmetric η^3-complex $[Cr(ox)_3]^{3-}$ or $[Fe(ox)_3]^{3-}$ serves as a complex-based ferromagnetic or ferrimagnetic building block which provides a three-dimensional network structure avoiding the very weak interchain interaction of traditional one-dimensional ferro- or ferrimagnetic materials (Pei *et al.*, 1991; Caneschi, Gatteschi, Rey & Sessoli, 1991). The compounds are designed such that the Cr^{III}/Fe^{III} and M^{II} ions are formed in alternate arrays over the three-dimensional lattice through bridging oxalato groups. The critical temperature can be linearly related to the amplitude of the magnetic interaction between Cr^{III}/Fe^{III} and M^{II} ions through the oxalato group. An oxalato-bridged Cr complex, $Na_2[N(CH_3)_3Ph]_5[Cr(ox)_3]_2.Cl.5H_2O$, has been reported recently (Farrell, Hambley & Lay, 1995) as the first member of a new class of microporous layer materials. Large cylindrical cavities are present within the layers of Na^+ and $[Cr(ox)_3]^{3-}$ ions. The size of the cavity is roughly 7 Å in diameter and 3 Å in depth and it is partially occupied by $N(CH_3)_3Ph^+$ templates. These templates can be removed either by cation exchange or by thermal methods without losing the crystallinity. Charge density studies of oxalic acid (Coppens, Sabine, Delaplane & Ibers, 1969; Stevens & Coppens, 1980; Dam, Harkema & Feil, 1983; Coppens *et al.*, 1984; Wang, Tsai, Liu & Calvert, 1985; Zobel, Luger, Dreissig & Koritsanszky, 1992) and its derivatives (Jovanovski, Thomas, Olovsson & Yugoslavia, 1988) have been widely investigated, so the ligand itself and in its acid form are well understood. The charge den-

Table 1. *Experimental details*

	Data set (I)	Data set (II)	Data set (III)
Crystal data			
Chemical formula	$C_4H_8NO_{10}Ti$	$C_4H_8NO_{10}Ti$	$C_4H_8NO_{10}Ti$
Chemical formula weight	278.1	278.1	278.1
Cell setting	Hexagonal	Hexagonal	Hexagonal
Space group	$P6_422$	$P6_422$	$P6_422$
a (Å)	8.939 (2)	8.931 (2)	8.947 (2)
c (Å)	10.893 (2)	10.893 (1)	10.898 (1)
V (Å^3)	753.7 (2)	752.4 (2)	755.4 (2)
Z	3	3	3
D_x (Mg m^{-3})	1.837	1.840	1.833
Radiation type	Mo $K\alpha$	Mo $K\alpha$	Ag $K\alpha$
Wavelength (Å)	0.7107	0.7107	0.5609
No. of reflections for cell parameters	25	24	25
θ range (°)	20–25	19–36	21–26
μ (mm^{-1})	0.84	0.84	0.46
Temperature (K)	298	130	298
Crystal form	Olive shaped	Olive shaped	Olive shaped
Crystal size (mm)	0.5 × 0.28 × 0.28	0.5 × 0.28 × 0.28	0.5 × 0.28 × 0.28
Crystal color	Black	Black	Black
Data collection			
Diffractometer	Nonius CAD-4	Nonius CAD-4	Nonius CAD-4
Data collection method	$\theta/2\theta$ scan width 2(0.70 + 0.35tan θ)° in 2θ, speed 2.06–8.24° min^{-1}	$\theta/2\theta$ scan width 2(0.70 + 0.35tan θ)° in 2θ, speed 2.06–8.24° min^{-1}	$\theta/2\theta$ scan width 2(0.70 + 0.45tan θ)° in 2θ, speed 2.06–8.24° min^{-1}
Absorption correction	Gaussian integration from crystal shape	Gaussian integration from crystal shape	Gaussian integration from crystal shape
T_{min}	0.74	0.74	0.85
T_{max}	0.84	0.84	0.87
No. of measured reflections	22 650	20 298	18 361
No. of independent reflections	4374	3699	3183
No. of observed reflections	3055	3170	2296
Criterion for observed reflections	$I > 2\sigma(I)$	$I > 2\sigma(I)$	$I > 2\sigma(I)$
R_{int}*	0.019	0.032	0.017
θ_{max} (°)	65	60	40
Range of h, k, l	$0 \rightarrow h \rightarrow 19$ $0 \rightarrow k \rightarrow 11$ $-26 \rightarrow l \rightarrow 27$	$0 \rightarrow h \rightarrow 17$ $0 \rightarrow k \rightarrow 10$ $-26 \rightarrow l \rightarrow 26$	$0 \rightarrow h \rightarrow 17$ $0 \rightarrow k \rightarrow 10$ $-23 \rightarrow l \rightarrow 24$
No. of standard reflections	4	3	3
Frequency of standard reflections	Every 2 h	Every 2 h	Every 2 h
Intensity decay (%)	±1	4	1
Refinement			
Refinement on	F	F	F
R†	0.031	0.025	0.035
wR‡	0.028	0.024	0.030
S§	1.82	2.68	1.86
No. of reflections used in refinement	3055	3170	2296
No. of parameters used	49	48	48
H-atom treatment	H atoms in calculated positions	H atoms in calculated positions	H atoms in calculated positions
Weighting scheme	$w = 1/[\sigma^2(F_o) + 0.00005F_o^2]$	$w = 1/[\sigma^2(F_o) + 0.00005F_o^2]$	$w = 1/[\sigma^2(F_o) + 0.00005F_o^2]$
$(\Delta/\sigma)_{max}$	0.001	0.001	0.001
$\Delta\rho_{max}$ (e Å^{-3})	0.57	0.56	0.69
$\Delta\rho_{min}$ (e Å^{-3})	−0.57	−0.74	−0.65
Extinction method	Secondary (Becker & Coppens, 1974)	None	None
Extinction coefficient	0.17 (3) × 10^{-4}	–	–
Source of atomic scattering factors	*International Tables for X-ray Crystallography* (1974, Vol. IV)	*International Tables for X-ray Crystallography* (1974, Vol. IV)	*International Tables for X-ray Crystallography* (1974, Vol. IV)

* $R_{int} = \Sigma|I_i - I_{av.}|/\Sigma I_i$. † $R = \Sigma(F_o = F_c)/\Sigma F_o$. ‡ $wR = [\Sigma w|F_o - F_c|^2/\Sigma wF_o^2]^{1/2}$. § $S = [\Sigma w|F_o - F_c|^2/(NR - NV)]^{1/2}$; NR = no. of reflections; NV = no. of variables.

sity of Ti^{4+} in the crystal of TiO_2 was studied by Shintani, Sato & Saito (1975) and Restori, Schwarzenbach & Schneider (1987). The influence of data reduction procedure, extinction correction, anharmonicity and radial parts of the multipole deformation function was investigated (Restori, Schwarzenbach & Schneider, 1987). The results show that a region of negative density at Ti, indicating an electron transfer, occurred from Ti to O. The structure, magnetic and spectral properties of the title compound have been reported recently (English & Eve, 1993), where the oxalato ion is tetradentate and is served as a bridging ligand between two Ti ions. The UV–vis spectrum displays two absorption bands at 13 500 and 5900 cm^{-1}, which was not readily assigned. The comparison in deformation densities of the oxalate dianion, oxalic acid and the form

in the tetradentate bridge ligand is also of interest. The crystals of the title compound are of good quality and have relatively low thermal parameters because of polymerization, therefore, it is reasonable to perform an accurate electron density study even at room temperature. Charge density studies of such a compound were performed at room temperature first using both Mo $K\alpha$ and Ag $K\alpha$ radiations. The extensive high-order reflections should affect the density distribution significantly in the region near the Ti nucleus and lone-pair electron. Unfortunately, the much weaker intensity of Ag $K\alpha$ radiation prevents the determination of unbiased nuclear thermal vibration. However, the same study was performed later at 130 K to ensure that the asphericity in the electron density around Ti would not be biased by the nuclear thermal vibration. We anticipate that the accurate mapping of the electron density in the vicinity of the Ti^{3+} center, which is supposedly a d^1 configuration, will lead to the correct splitting of d orbitals in the D_4 crystal field. This may provide a feasible explanation for the spectral feature.

Table 2. *Fractional atomic coordinates and equivalent isotropic displacement parameters (Å²)*

$$B_{eq} = (8\pi^2/3)\Sigma_i\Sigma_j U_{ij} a_i^* a_j^* \mathbf{a}_i.\mathbf{a}_j.$$

	x	y	z	B_{eq}
Data set (I)				
Ti	1.0	1/2	0.83333	0.831 (4)
O1	0.76296 (7)	0.44900 (7)	0.72365 (6)	1.54 (1)
O2	0.92389 (6)	0.27249 (6)	0.72987 (5)	1.34 (1)
O3	0.7502 (2)	0.7502 (2)	2/3	4.21 (5)
C1	0.69175 (3)	0.30825 (3)	2/3	1.09 (2)
C2	0.78951 (3)	0.21049 (3)	2/3	1.00 (1)
N	0.0	0.0	0.16667	3.64 (6)
Data set (II)				
Ti	1.0	1/2	0.83333	0.410 (4)
O1	0.76287 (6)	0.44938 (6)	0.72385 (5)	0.74 (1)
O2	0.92462 (6)	0.27273 (6)	0.72991 (4)	0.67 (1)
O3	0.7493 (1)	0.7493 (1)	2/3	1.70 (2)
C1	0.69163 (4)	0.30837 (4)	2/3	0.55 (1)
C2	0.78975 (4)	0.21025 (4)	2/3	0.53 (1)
N	0.0	0.0	0.16667	1.66 (3)
Data set (III)				
Ti	1.0	1/2	0.83333	0.872 (6)
O1	0.7629 (1)	0.4489 (1)	0.72371 (9)	1.60 (2)
O2	0.9239 (1)	0.2724 (1)	0.73001 (8)	1.38 (2)
O3	0.7503 (3)	0.7503 (3)	2/3	4.36 (6)
C1	0.69173 (6)	0.30867 (6)	2/3	1.14 (2)
C2	0.78948 (5)	0.21052 (5)	2/3	1.03 (2)
N	0.0	0.0	0.16667	3.74 (7)

2. Experimental

2.1. *Data collection*

The title compound, $NH_4[Ti(C_2O_4)_2].2H_2O$, was prepared from $TiCl_3.6H_2O$ in oxalic acid dihydrate aqueous solution according to the literature (English & Eve, 1993). Suitable crystals were grown from aqueous solution. A crystal was selected and sealed in a 0.5 mm capillary for intensity data measurement. Experimental details are given in Table 1. For data set (I), intensity data of five equivalent sets ($+h$ $+k$ $\pm l$, $-h$ $+k$ $\pm l$, $+h$ $-k$, $\pm l$) were measured for $\sin\theta/\lambda$ up to 1.275 $Å^{-1}$. In addition, four equivalent sets of reflections with azimuth angles ψ = 30, 10, −10 and −30° were collected for each unique reflection ($+h$, $+k$, ± 1) up to $\sin\theta/\lambda$ of 0.704 $Å^{-1}$. An absorption correction (Alcock, 1969) was applied by 18 measured faces.

2.2. *Multipole refinement*

In addition to the conventional least-squares refinement, a multipole refinement (Hansen & Coppens, 1978) was applied with a multipole expansion of the valence shell up to hexadecapoles for the Ti, O and C atoms and up to dipoles for the H atoms. Hartree–Fock functions were used for the monopoles. Scattering factor tables of both core and valence electrons were taken from *International Tables for X-ray Crystallography* (1974, Vol. IV). Hydrogen positions were fixed by elongating along the bond axis to bond lengths of N—H 1.03 and O—H 1.00 Å, respectively (Allen *et al.*, 1987). The coefficients of all the multipole terms, together with positional and anisotropic thermal parameters of non-H atoms, were obtained by full-matrix least-squares refinement based on F. The core-electron configurations were assumed to be Ar for Ti and He for C, N and O. The total charge of the crystal was kept neutral. Since Ti, C1, C2 and N atoms are all at special positions with site symmetries 222± for Ti and N and 2− for C1 and C2, therefore, the number of refined multipole coefficients for the former is 7 and for the latter 13. An isotropic secondary extinction correction (Becker & Coppens, 1974) was included in the refinement of data set (I); but not for data sets (II) and (III). *NRCVAX* (Gabe, Le Page, Charland, Lee & White, 1989) was used for structure analysis. Multipole refinement was performed with the *MOLLY* program (Hansen & Coppens, 1978).

2.3. *Deformation-density maps*

Two types of multipole model deformation density maps are presented in this work. The first is a dynamic model density, $\Delta\rho_{m-a}$, where the electron density is calculated *via* Fourier synthesis. The Fourier coefficients are obtained from the difference between two F_c values, including the thermal vibrations – one derived from a multipole model with a series expansion of spherical harmonics (Hansen & Coppens, 1978), the other being the spherical part of the model density. The second is a static model density, $\Delta\rho_{m-a,\text{static}}$, which is calculated in the direct space according to the multipolar model (Hansen & Coppens, 1978) without taking into account the nuclear thermal vibration. The deformation density maps are produced by a locally developed contour-plotting program (Tsai, 1982).

Table 3. *Agreement indices from multipole refinements*

Data sets (*a*) (I), (*b*) (II) and (*c*) (III).

		NV	*R*	*wR*	R_2	wR_2	*S*	*g*
Spherical	(*a*)	41	0.033	0.045	0.045	0.071	2.892	0.17 (3) $\times 10^{-4}$
neutral	(*b*)	40	0.027	0.036	0.046	0.067	2.354	0
	(*c*)	40	0.038	0.052	0.053	0.076	3.214	0
Monopole	(*a*)	54	0.030	0.025	0.035	0.036	1.610	0.17 (3) $\times 10^{-4}$
	(*b*)	53	0.024	0.024	0.036	0.041	1.590	0
	(*c*)	53	0.034	0.027	0.038	0.036	1.652	0
Hexadecapole	(*a*)	156	0.025	0.017	0.025	0.022	1.123	0.17 (3) $\times 10^{-4}$
	(*b*)	155	0.021	0.020	0.031	0.034	1.315	0
	(*c*)	155	0.029	0.019	0.028	0.023	1.183	0

$R_2 = \Sigma(F_o^2 - F_c^2)/\Sigma F_o^2$. $wR_2 = [\Sigma w|F_o^2 - F_c^2|^2/\Sigma wF_o^4]^{1/2}$. *NV*, *R*, *wR*, *S* and *g* are defined as in Table 1.

3. Results and discussion

Atomic parameters from three data sets based on the hexadecapole refinement are listed in Table 2.* The bond lengths and angles for three data sets are within the deviation. Agreement indices for full-matrix least-squares refinements based on the multipole model are listed in Table 3. Each Ti atom is coordinated to four bidentate oxalato ligands and forms a square antiprism with approximate D_{4d} symmetry (Fig. 1). Each oxalate ion is served as a bridge between two Ti atoms and forms a very interesting spiral column along the *c* axis. NH_4^+ and H_2O are packed together with hydrogen bonding and form a rod-like column surrounded by the Ti oxalato spiral columns. Since the space group of the compound is noncentrosymmetric, the usual experimental deformation density map ($\Delta\rho_{x-x}$) cannot be properly represented because of the phase difference yield from the model of full data refinement and the model of high-order refinement. The importance of the phase improvement for the deformation study was pointed out by Morooka, Ohba & Miyamae (1992). Therefore, here we only present the model deformation density maps – dynamic and static. The multipole model deformation density map of the plane with one bridging oxalato ligand and two Ti atoms is shown in Fig. 2. Positive density accumulations are found at the midpoints of the C—C and C—O bonds; lone-pair electrons at O are clearly observable. The peak density along the C2—O2 bond is slightly higher than that along the C1—O1 bond. This result is consistent with the bond lengths of the oxalato ligand, where C2—O2 [1.2483 (5) Å] is shorter than C1—O1 [1.2540 (5) Å]. The dianion has a twofold axis along C1—C2, with the general feature in deformation density of this anion being quite similar to that of the acid form (Wang, Tsai, Liu & Calvert, 1985; Dam, Harkema & Feil, 1983). Concurrently, the bond length Ti— O1 [2.2713 (5) Å] is significantly longer than Ti—O2 [2.1178 (5) Å] and the corresponding density around O2 toward Ti is somewhat larger than that around O1 (Fig. 2). From this deformation density map, it can be described that the oxalato ligand is a dianion form, $C_2O_4^{2-}$, which is bridged between two Ti atoms. The bonding of Ti—O is of a dative bond fashion, *i.e.* with the lone-pair electron of the O atom donated to the Ti ion. There is a slight difference in density on the two O atoms (O1 and O2). The residual density map for data (II) is shown in Fig. 2(*g*); no significant feature is found in this map. In order to see clearly the asphericity in density around Ti, two more planes are plotted – one with O1—Ti—O1^i and the other O2—Ti—O2^i. Such deformation densities from data (II) are shown in Figs. 3 and 4. The figures of the other two data sets are essentially the same and are not included here.* These two planes are quite similar, except the density around O2 is slightly greater than that around O1 mentioned above. There is positive density accumulation around the Ti atom in the direction at bisection of ∠ O1—

* See deposition footnote.

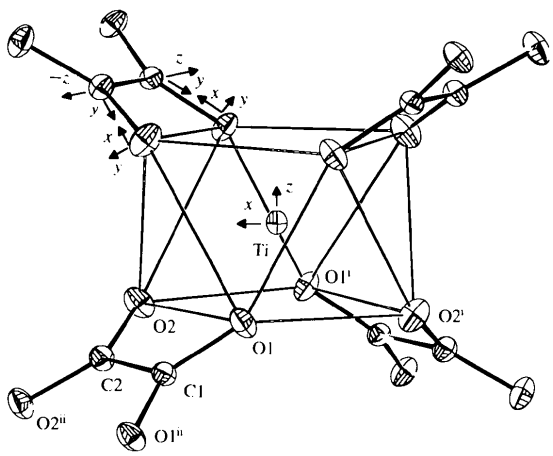

Fig. 1. Molecular drawing with thermal ellipsoids (50% probability) at room temperature and choice of local Cartesian axes for the multipole refinements. Symmetry codes: (i) $2 - x, 1 - y, z$; (ii) $1 - y, 1 - x, \frac{4}{3} - z$.

* Lists of structure factors, anisotropic displacement parameters, H-atom coordinates and multipole coefficients, and deformation density maps for data sets (I) and (III) have been deposited with the IUCr (Reference: AS0695). Copies may be obtained through The Managing Editor, International Union of Crystallography, 5 Abbey Square, Chester CH1 2HU, England.

Ti—O1^i and ∠ O2—Ti—O2^i. It is obvious (Figs. 2, 3 and 4) that along the σ-bond direction ($d\sigma$), there is always depletion of density around the Ti atom. This indicates that the bonding orbital of Ti—O is mainly contributed from the O atom, which indicates a somewhat stronger ionic character in such a bond. A similar phenomenon was also found in TiO_2 (Restori, Schwarzenbach & Schneider, 1987). Each Ti atom in TiO_2 is octahedrally bonded with two long axial Ti—O bonds [1.9800 (9) Å] and four short equatorial Ti—O bonds [1.9485 (5) Å]. The deformation density maxima along the Ti—O bonds are located near the O atoms. The negative deformation density at Ti may be explained as due to the ionic character of such a bond, indicating electron transfer from Ti to O. However, in the bond diagonal directions ($d\pi$), unlike the Ti atom

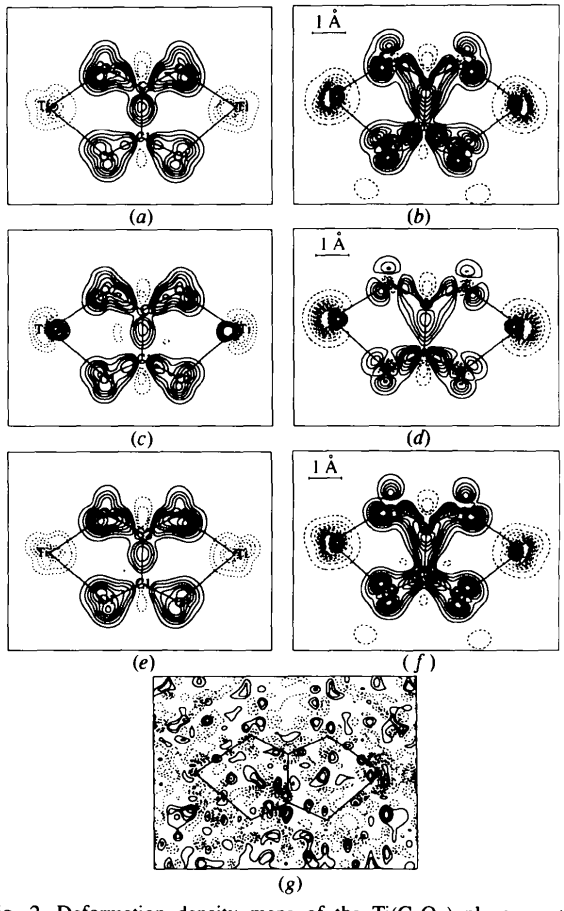

Fig. 2. Deformation density maps of the $Ti(C_2O_4)$ plane; contour interval 0.1 within ± 1.0 e Å^{-3}; solid line positive, dashed line negative. (*a*) $\Delta\rho_{m-a}$ (I); (*b*) $\Delta\rho_{m-a,\text{static}}$ (I); (*c*) $\Delta\rho_{m-a}$ (II); (*d*) $\Delta\rho_{m-a,\text{static}}$ (II); (*e*) $\Delta\rho_{m-a}$ (III); (*f*) $\Delta\rho_{m-a,\text{static}}$ (III); (*g*) residual density map (II). The standard deviations are 0.15, 0.12 and 0.16 e Å^{-3} for data sets (I), (II) and (III) in the general position.

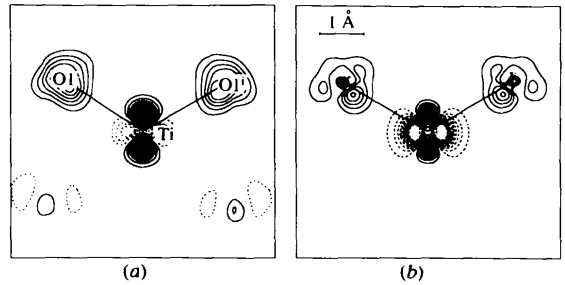

Fig. 3. Deformation density maps of the O1—Ti—O1^i plane: (*a*) $\Delta\rho_{m-a}$ (II); (*b*) $\Delta\rho_{m-a,\text{static}}$ (II). Contours are defined as in Fig. 2.

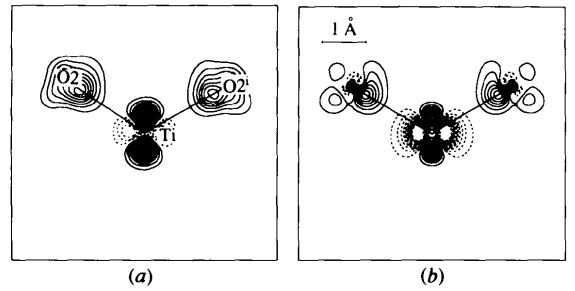

Fig. 4. Deformation density maps of the O2—Ti—O2^i plane: (*a*) $\Delta\rho_{m-a}$ (II); (*b*) $\Delta\rho_{m-a,\text{static}}$ (II). Contours are defined as in Fig. 2.

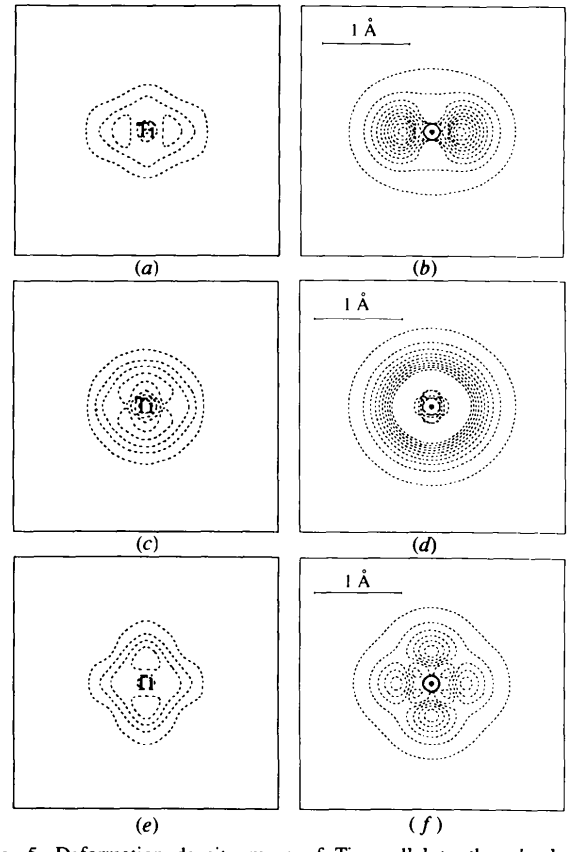

Fig. 5. Deformation density maps of Ti parallel to the *ab* plane: (*a*) $\Delta\rho_{m-a}$ (I); (*b*) $\Delta\rho_{m-a,\text{static}}$ (I); (*c*) $\Delta\rho_{m-a}$ (II); (*d*) $\Delta\rho_{m-a,\text{static}}$ (II); (*e*) $\Delta\rho_{m-a}$ (III); (*f*) $\Delta\rho_{m-a,\text{static}}$ (III). Contours are defined as in Fig. 2.

Table 4. *Net atomic charges (e) of* $NH_4[Ti(C_2O_4)_2].2H_2O$ *from monopole refinement*

Data sets (*a*) (I), (*b*) (II) and (*c*) (III).

	Ti	O1	O2	O3	N	C1	C2	H1	H2	Fragments NH_4	Fragments C_2O_4	Fragments H_2O
(*a*)	1.80 (2)	−0.42 (3)	−0.67 (3)	−0.54 (2)	−1.00 (3)	0.26 (2)	0.44 (3)	0.36 (3)	0.45 (4)	0.44	−1.48	0.36
(*b*)	1.96 (2)	−0.42 (2)	−0.57 (2)	−0.70 (2)	−0.96 (3)	0.30 (2)	0.38 (2)	0.36 (2)	0.40 (3)	0.48	−1.30	0.10
(*c*)	2.12 (1)	−0.52 (3)	−0.73 (3)	−0.64 (2)	−1.00 (3)	0.36 (3)	0.54 (3)	0.34 (3)	0.51 (4)	0.36	−1.60	0.38

Table 5. *The d-orbital populations of Ti from multipole refinements*

Data sets (*a*) (I), (*b*) (II) and (*c*) (III).

	d_{z^2}	$d_{x^2-y^2}$	d_{xy}	d_{yz}	d_{xz}
(*a*)	0.70 (43%)	0.20 (13%)	0.25 (16%)	0.18 (11%)	0.27 (17%)
(*b*)	0.74 (38%)	0.14 (7%)	0.15 (7%)	0.47 (24%)	0.47 (24%)
(*c*)	0.66 (43%)	0.18 (12%)	0.28 (18%)	0.17 (11%)	0.25 (16%)

in TiO_2, there is positive deformation density along the pseudofourfold axis <001>, indicating a greater electron population in the d_{z^2} orbital than the other *d* orbitals at Ti (Figs. 3 and 4). The deformation density map of the plane perpendicular to this pseudofourfold axis containing Ti (*xy* plane) is shown in Fig. 5. The $\Delta\rho$ maps derived from data sets (II) and (III) (Figs. 5*c* and *e*) and (I) (Fig. 5*a*) are all negative, but slightly different in shape. These maps should reflect electron populations on $d_{x^2-y^2}$ and d_{xy} orbitals. It is understandable that the deformation density at the region very close to the nucleus (within 0.8 Å) often suffered from large error (Restori, Schwarzenbach & Schneider, 1987). Unfortunately, this is the most interesting region around the transition metal. In general, deformation densities from data sets (I), (II) and (III) are very similar, with only small differences near the Ti nucleus. It is worth noting that data set (III) is much less affected by absorption and extinction.

According to the simple crystal-field theory, when Ti is a square antiprism, D_4 (Parish & Perkins, 1967), d_{xz} and d_{yz} orbitals are degenerate (e_3) and are the highest in energy among all *d* orbitals, since only these two orbitals are eligible for the σ-bond. d_{xy} and $d_{x^2-y^2}$ are also degenerate (e_2) and are lower in energy than e_3. The d_{z^2} orbital (a_1) is in the lowest energy level. The latter three a_1 and e_2 orbitals are all nonbonding orbitals. Thus, the supposedly one *d* electron in Ti^{3+} should be mostly populated at the d_{z^2} orbital, which is in accordance with our observation. The diffuse reflectance spectra observed at 13 500 and 5900 cm^{-1} (English & Eve, 1993) could be due to the electron transitions between d_{z^2} and (d_{xz}, d_{yz}) and (d_{xy}, $d_{x^2-y^2}$) orbitals. The populations among the five *d* orbitals are such that the d_{z^2} orbital is most populated and the remaining *d* orbitals are more or less evenly distributed (Table 5). The asphericity in deformation density around the Ti atom is quite clear and conforms to the prediction of simple crystal-field theory.

Hydrogen bonds play an important role in this crystal. Two types of hydrogen bonds are found in the title compound. One hydrogen bond is between NH_4^+ and H_2O and the other is between O1 of the oxalato ligand and H_2O. Deformation density maps of N—H1···O3 and O3—H2···O1 from data set (II) are shown in Figs. 6 and 7. The lone-pair electrons of O3 (H_2O) and O1 are clearly polarized toward the H-atom direction. The distances of N···O3 and O3···O1 are 2.882 (1) and 2.811 (1) Å, respectively. There is no hydrogen bond around the O2 atom. This may be the reason for the significantly shorter distance of Ti—O2 than Ti—O1.

The net atomic charge of each atom and the charge of each fragment are given in Table 4. Atomic charges show slight differences in all three data sets. According to the fragment charge, the NH_4^+ ion is *ca* +0.5, the oxalato ligand is −1.5, the expected neutral H_2O molecule is +0.3 and the Ti^+ ion is +2.0. It is worth noting

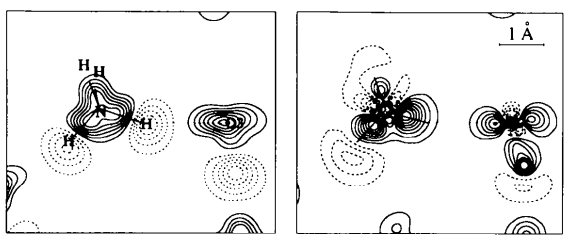

(*a*) (*b*)

Fig. 6. Deformation density maps of N—H1···O3: (*a*) $\Delta\rho_{m-a}$ (II); (*b*) $\Delta\rho_{m-a,\text{static}}$ (II). Contours are defined as in Fig. 2.

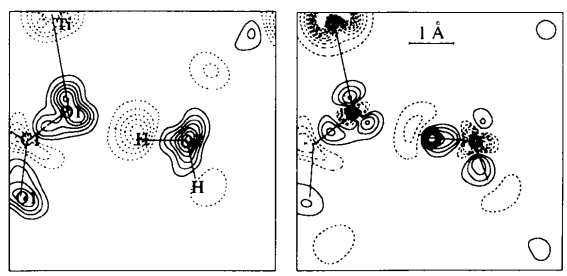

(*a*) (*b*)

Fig. 7. Deformation density maps of O3—H2···O1: (*a*) $\Delta\rho_{m-a}$ (II); (*b*) $\Delta\rho_{m-a,\text{static}}$ (II). Contours are defined as in Fig. 2.

that two C and two O atoms (C1, C2 and O1, O2) in the oxalato ligand carry quite different charges, respectively, where O2 is more negative than O1 and C2 is more positive than C1. This may have the consequence that only O1 is hydrogen bonded to H_2O. Such a slightly uneven charge distribution is also detectable in the deformation density shown in Fig. 2.

Thanks are due to the National Science Council of the Republic of China for the financial support of this work.

References

Alcock, N. W. (1969). *Acta Cryst.* A**25**, 518–520.

Allen, F. H., Kennard, O., Watson, D. G., Brammer, L., Orpen, A. G. & Taylor, R. (1987). *J. Chem. Soc. Perkin Trans. 2*, pp. S1–S18.

Becker, P. & Coppens, P. (1974). *Acta Cryst.* A**30**, 129–147.

Bulc, N., Golic, L. & Siftar, J. (1983). *Acta Cryst.* C**39**, 176–178.

Caneschi, A., Gatteschi, D., Rey, P. & Sessoli, R. (1991). *Inorg. Chem.* **30**, 3936–3941.

Chaix-Pluchery, O., Mutin, J. C., Bouillot, J. & Niepce, J. C. (1989). *Acta Cryst.* C**45**, 1699–1705.

Christensen, A. N., Cox, D. E. & Lehmann, M. S. (1989). *Acta Chem. Scand.* **43**, 19–25.

Coppens, P., Dam, T., Harkema, S., Feil, D., Feld, R., Lehmann, M. S., Goddard, R., Kruger, C., Hellner, E., Johansen, H., Larsen, F. K., Koetzle, T. F., McMullan, R. K., Maslen, E. N. & Stevens, E. D. (1984). *Acta Cryst.* A**40**, 184–195.

Coppens, P., Sabine, T. M., Delaplane, R. G. & Ibers, J. A. (1969). *Acta Cryst.* B**25**, 2451–2458.

Curtis, N. F., Ross, I., McCormick, N. & Waters, T. N. (1973). *J. Chem. Soc. Dalton Trans.* pp. 1537–1548.

Dam, T., Harkema, S. & Feil, D. (1983). *Acta Cryst.* B**39**, 760–768.

Drew, M. G. B. & Eve, D. J. (1977*a*). *Inorg. Chim. Acta*, **25**, L111–L112.

Drew, M. G. B. & Eve, D. J. (1977*b*). *Acta Cryst.* B**33**, 2919–2921.

English, R. B. & Eve, D. J. (1993). *Inorg. Chim. Acta*, **203**, 219–222.

Eve, D. J. & Niven, M. L. (1990). *Inorg. Chim. Acta*, **174**, 205–208.

Farrell, R. P., Hambley, T. W. & Lay, P. A. (1995). *Inorg. Chem.* **34**, 757–758.

Felthouse, T. R., Laskowski, E. J. & Hendrickson, D. N. (1977). *Inorg. Chem.* **16**, 1077–1089.

Gabe, E. J., Le Page, Y., Charland, J.-P., Lee, F. L. & White, P. S. (1989). *J. Appl. Cryst.* **22**, 384–387.

Hansen, N. K. & Coppens, P. (1978). *Acta Cryst.* A**34**, 909–921.

Huang, S. H., Wang, R. J. & Thomas, C. W. M. (1990). *J. Cryst. Spectrosc. Res.* **20**, 99–104.

Jovanovski, G., Thomas, J. O., Olovsson, I. & Yugoslavia, S. (1988). *Z. Krist.* **185**, 654.

Julve, M., Verdaguer, M., Gleizes, A., Philoche-Levisalles, M. & Kahn, O. (1984). *Inorg. Chem.* **23**, 3808–3818.

Morooka, M., Ohba, S. & Miyamae, H. (1992). *Acta Cryst.* B**48**, 667–672.

Ohba, M., Tamaki, H., Matsumoto, N. & Okawa, H. (1993). *Inorg. Chem.* **32**, 5385–5390.

Parish, R. V. & Perkins, P. G. (1967). *J. Chem. Soc. A*, pp. 345–348.

Pei, Y., Kahn, O., Nakatani, K., Codjovi, E., Mathoniere, C. & Sletten, J. (1991). *J. Am. Chem. Soc.* **113**, 6558–6564.

Restori, R., Schwarzenbach, D. & Schneider, J. R. (1987). *Acta Cryst.* B**43**, 251–257.

Shintani, H., Sato, S. & Saito, Y. (1975). *Acta Cryst.* B**31**, 1981–1982.

Stevens, E. D. & Coppens, P. (1980). *Acta Cryst.* B**36**, 1864–1876.

Tamaki, H., Mitsumi, M., Nakamura, K., Matsumoto, N., Kida, S., Okawa, H. & Iijima, S. (1992). *Chem. Lett.* pp. 1975–1978.

Tamaki, H., Zhong, Z. J., Matsumoto, N., Kida, S., Koikawa, M., Achiwa, N., Hashimoto, Y. & Okawa, H. (1992). *J. Am. Chem. Soc.* **114**, 6974–6979.

Tsai, C. J. (1982). MSc thesis. National Taiwan University, Taiwan.

Virovets, A. V., Naumov, D. Y., Boldyreva, E. V. & Podberezskaya, N. V. (1993). *Acta Cryst.* C**49**, 1882–1884.

Wang, Y., Tsai, C. J., Liu, W. L. & Calvert, L. D. (1985). *Acta Cryst.* B**41**, 131–135.

Zhong, Z. J., Matsumoto, N., Okawa, H. & Kida, S. (1990). *Chem. Lett.* pp. 87–90.

Zobel, D., Luger, P., Dreissig, W. & Koritsanszky, T. (1992). *Acta Cryst.* B**48**, 837–848.